Behavioral Modeling of Resonant Power Transfer Systems with Capacitive Coupling: Two-Port Network Approach

Eli Abramov, *Student Member*, *IEEE*,
Mor Mordechai Peretz, *Member*, *IEEE*

The Center for Power Electronics and Mixed-Signal IC,
Department of Electrical and Computer Engineering
Ben-Gurion University of the Negev
P.O. Box 653, Beer-Sheva 8410501, Israel
eliab@post.bgu.ac.il, morp@bgu.ac.il
http://www.ee.bgu.ac.il/~pemic

Ilya Zeltser, Member, *IEEE*

Power Electronics Department
Rafael Advanced Defense Systems Ltd.
P.O. Box 2250, Haifa 31021, Israel
ilyaz@rafael.co.il
www.rafael.co.il

***Abstract* — In this paper, a network based approach to model resonant conversion systems with capacitive coupling is introduced. The modeling methodology provides an efficient tool to investigate capacitive-based wireless power transfer (WPT) systems, in particular for the output characteristics under variations of the components and the coupling parameters. The model enables to explore the dynamics as well as the intricate interactions between the multiple parameters of the systems that can be translated into guidelines in the design of compensators and operation in closed-loop. In addition, a simulation-compatible model of the capacitive coupler using a continuous-time variable capacitor has been constructed in order to provide a simulation framework for the analysis of capacitive-based WPT systems under medium variations. To validate the modeling approach, an experimental capacitive WPT prototype operating at the MHz range has been designed and examined for various air-gaps. The experimental results of the prototype are in excellent agreement with the theoretical analysis and simulations.**

Keywords* — *capacitive power transfer, matching networks, modeling, two-port network, simulation-compatible model.

I. Introduction

As the field of mobile technology advances and adds more innovative uses, applications such as portable electronics, virtual and augmented reality, smartphones, electric vehicles, biomedical systems, etc. are being used for extended periods, ideally continuously [1]-[6]. With increasing computing power to support the technology ramp-up, mobile power, essential to keep the high-performance devices available at all times, becomes more desirable. Technology of wireless power transfer (WPT) is one of the promising reliable sources of energy to reduce dependency of weight-sensitive or volume-sensitive mobile and portable applications on bulk batteries [6]-[12].

Capacitive power transfer (CPT) has been investigated in recent years, as an alternative near-field power transfer method to well-known magnetic-field-based approaches [1], [6]-[9] . One of the more attractive advantages of capacitive-based WPT is the avoidance of undesired Eddy currents and electromagnetic interference (EMI) that come with magnetic-based WPT methods. In addition to efficiency improvements, CPT systems are potentially with lower volume and construction complexity [13]-[18]. However, the power transfer capability and efficiency still depends on the distance and alignment between the transmitting and receiving sides, which is an inherent feature of near-field WPT systems [14], [18], [19]. Several explorations and remedies for an extended range power transfer are covered in the literature [20]-[22], for general and capacitive power transfer. An important step in the development of both uniform and specific solutions for extended range WPT systems is a generalized description of the energy transfer mechanism. This requires description of the transfer medium, circuit behavior and their interaction. In particular, in case that active compensation is applied, a description of the system's dynamic response is essential. On the topic of magnetic field-based WPT, there can be found several models based on circuit and system analyses, however, a generic behavioral model and modeling methodology for CPT has not been addressed hitherto.

A simplified block diagram of a descriptive CPT system is shown in Fig. 1, there, similarly to magnetic-field-based WPT approaches, reactive networks on both primary and secondary sides are used for impedance matching between the source and load [21]-[23]. To achieve suitable degrees of freedom in terms of design, performance and overall input-output relationships in any WPT system, high-order matching networks are used [14], [21]-[24]. Analysis of such high-order networks can be quite complex and tedious. As a result, the complex interaction between the system parameters and characteristics may be overlooked. Several approaches have been employed to decipher the operation of high-order resonant structures such as: analytical multivariable matrix manipulations, geometrical representations [25], [26], and averaging [26]-[28]. Numerical simulations are also a strong tool to evaluate and characterize different resonant circuits. This approach however, loses

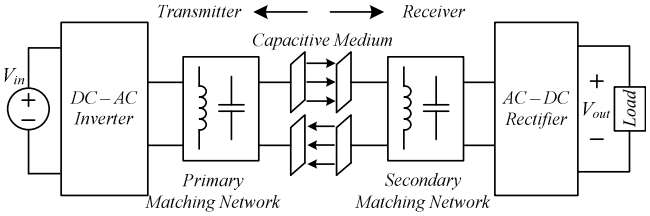

Fig. 1. Typical diagram of capacitive WPT system.

generality and may be time consuming for cases that a time domain cycle-by-cycle simulation for high-frequency drive signals (several MHz) is carried out [30]-[33].

The objective of this study is to introduce a two-port network approach to describe the behavior of resonant-based capacitive WPT system for various operating conditions. The presented network-based modeling methodology leads to a unified approach, that enables to account for the cross-coupling relationship between the input and output parameters. It is a further objective of this study to present a simulation-compatible model of the capacitive coupling based on a continuous-time variable capacitor representation. This provides simulation platform to further analyze and examine resonant wireless CPT.

The rest of the paper is organized as follows. Section II details two-port network-based analysis. Section III presents a case study of a network-based approach to analyze a resonant capacitive WPT. Section IV describes a simulation-compatible model of capacitive coupling medium using a continuous variable capacitor. Experimental validation of the behavioral model is provided in Section V. Finally, Section VI concludes the paper.

II. Equivalent Representations of Matching Networks

A fundamental building block of various resonant conversion systems is a matching network. It typically comprises a second or higher order impedance that connects a sourcing circuit to a loading one. The use of these networks serves many design objectives such as reducing circulating energy in the converter [34], lowering voltage and current stresses of the switches, assuring soft-switching over wide range [21], etc. Particularly in WPT systems, matching networks provide additional degrees of freedom to interact between the primary and secondary circuits and compensate for: resonant frequency, Volt-Ampere ratings, constant voltage/current output (load-independent operation), output power and system efficiency [18], [21]-[23]. This section, which briefly reviews some of the basic matching networks, is carried out in the particular context of capacitive wireless medium. The latter is then used to characterize the behavior of a network as an energy transfer element.

Matching L-type structures such as series inductor combined with parallel capacitor and parallel capacitor combined with series inductor are typically used in various WPT systems [16], [18], and can be described by a two-port network with gyrator characteristics [36]. A gyrator is a passive, lossless, linear two-port transformation network in which the output and input currents depend on the input and output voltages, in accordance, with respect to its transconductance gain G. In circuit theory, gyrators are often used to emulate inductance using capacitance, transform impedance into admittance, and vice versa [37]. The input-output relationship of an ideal gyrator as a two-port network can be expressed as

$$\begin{bmatrix} I_1 \\ I_2 \end{bmatrix} = \begin{bmatrix} 0 & -G \\ G & 0 \end{bmatrix} \begin{bmatrix} V_1 \\ V_2 \end{bmatrix}. \tag{1}$$

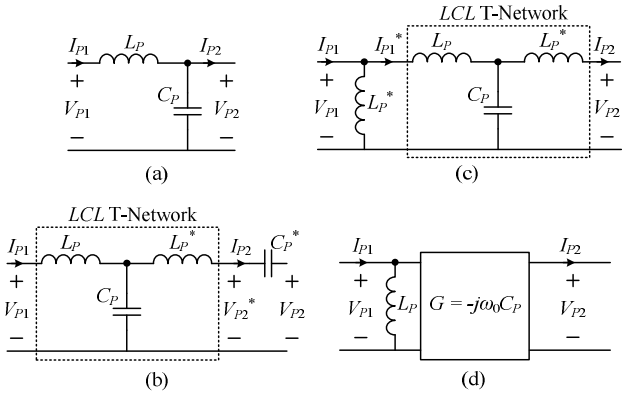

Fig. 2. Equivalent representations of series-parallel *LC* matching network: (a) L-type series-parallel resonant *LC* circuit; (b) Series resonator connected to the L-type circuit for T-type network arrangement; (c) Modified T-type series-parallel *LC* resonant circuit; (d) Two-port network with gyrator characteristics.

In the context of the above discussion, voltage and current relationships of a series-parallel *LC* matching structure (Fig. 2a) can be derived as follows

$$\begin{cases} V_{P1} = j\omega L_P I_{P1} + V_{P2} \\ V_{P2} = \dfrac{1}{j\omega C_P}\left(I_{P1} - I_{P2}\right) \end{cases} \Rightarrow \begin{cases} I_{P1} = \dfrac{\left(V_{P1} - V_{P2}\right)}{j\omega L_P} \\ V_{P1} = j\omega L_P I_{P1} + \dfrac{1}{j\omega C_P}\left(I_{P1} - I_{P2}\right) \end{cases}. \tag{2}$$

Assuming operation at the resonant frequency, the currents I_{p1} and I_{p2} are given by

$$\begin{cases} I_{P1} = -j\omega_0 C_P \left(V_{P1} - V_{P2}\right) \\ I_{P2} = -j\omega_0 C_P V_{P1} \end{cases} ; \quad \omega_0 L_P = \frac{1}{\omega_0 C_P}, \tag{3}$$

where ω_0 is the resonant angular frequency.

Employing few configurational modifications to the L-type network of Fig. 2a, while staying at resonant frequency, an equivalent representation can be obtained. As can be seen in Fig. 2b, by addition of a series resonator (whereas $L_P^* = L_P$ and $C_P^* = C_P$) the network is transformed into a T-type one (L_P-C_P-L_P^*) with an output series capacitance C_P^*. The resultant voltage and current relationships have a two-port gyrator characteristics as follows:

$$\begin{aligned} V_{P1} &= j\omega_0 L_P I_{P1} + \frac{1}{j\omega_0 C_P}\left(I_{P1} - I_{P2}\right) = \frac{1}{-j\omega_0 C_P} I_{P2} \\ V_{P2}^* &= -j\omega_0 L_P I_{P2} + \frac{1}{j\omega_0 C_P}\left(I_{P1} - I_{P2}\right) = \frac{1}{j\omega_0 C_P} I_{P1} \end{aligned}, \tag{4}$$

and in matrix representation, (4) can be written as

$$\begin{bmatrix} I_{P1} \\ I_{P2} \end{bmatrix} = \begin{bmatrix} 0 & \underbrace{j\omega_0 C_P}_{-G} \\ \underbrace{-j\omega_0 C_P}_{G} & 0 \end{bmatrix} \begin{bmatrix} V_{P1} \\ V_{P2}^* \end{bmatrix}, \tag{5}$$

where the transconductance gain is $G = -j\omega_0 C_P$. It should be noted that since operation in resonance is assumed, the addition of the series branch is effectively short circuit and does not change the circuit's behavior.

Following the above observations, the series output capacitance C_P^* can be reflected to an input parallel inductance L_P^*, as shown in Fig. 2c. Finally, the original L-type network can be represented as a gyrator element (Fig. 2d) with parallel input inductance L_p.

In analogy to the above practice for the series-parallel *LC* matching network, the parallel-series *LC* structure in Fig. 3a can also be defined by gyration ratio. This is facilitated by addition of a parallel resonator (whereas $L_P^* = L_P$ and $C_P^* = C_P$) as shown in Fig. 3b. Similarly to the case of the series branch, the parallel resonator is effectively open circuit when operating at resonance and does not change the original characteristics of the circuit. The L-network is transformed into a π-type one (C_S-L_S-C_S^*) with parallel output inductor L_S^*. The parallel-series *LC* structure can be described as a gyrator element with parallel output inductor L_S as shown in Fig. 3c.

III. Case Study: Capacitive Wireless Power Transfer System

Following the observations and derivations made in the previous section, a capacitively-coupled power transfer system with double-sided L-type matching networks is analyzed. The schematic diagram of the full system is shown in Fig. 4. This configuration has been selected for the case study demonstration since it has been widely employed in a variety of medium power level CPT applications [16], [18]. As can be seen in Fig. 6, the matching networks are a series-parallel *LC* circuit at the primary and a parallel-series *LC* at the secondary. The capacitive medium is modeled by a π-network, such that C_M is the equivalent mutual capacitance and C_{M1} and C_{M2} are the self-capacitances of the coupling plates [15], [16]. The system is driven by a full-bridge inverter on the primary side, and the load is fed via a diode rectifier that is connected to the secondary's network. Due to the structural constraints of the coupling plates, as a general practice, it is assumed that the coupling capacitance C_M is significantly lower than the total parallel capacitance. Consequently, the driving frequency is near the matching networks' resonant frequency (i.e., $f_0=1/(2\pi\sqrt{L_P C_P}) = 1/(2\pi\sqrt{L_S C_S})$). Since high-Q operation is naturally obtained by the high output impedance of the primary's network, the currents as well as voltages of the reactive elements are virtually sinusoidal.

For the derivations of the model, the circuit of Fig. 4 is simplified by separating the parallel capacitances of the medium from the model's self-capacitances, as shown in Fig. 5a. This forms a π-network constructed by the mutual capacitance C_M, which can be analyzed similarly to the *CLC* π-matching network from Section II. This enables to use a gyrator element to represent the coupling behavior, as depicted in Fig. 5b. In the context of the overall system, Fig. 4 is simplified as delineated in Fig. 5c (where $C_P >> C_{M1}$ and $C_S >> C_{M2}$). Applying the network dualities that have been established earlier, the entire system is represented by three gyrators connected in series, as shown in Fig. 5d. This is further reduced to a single

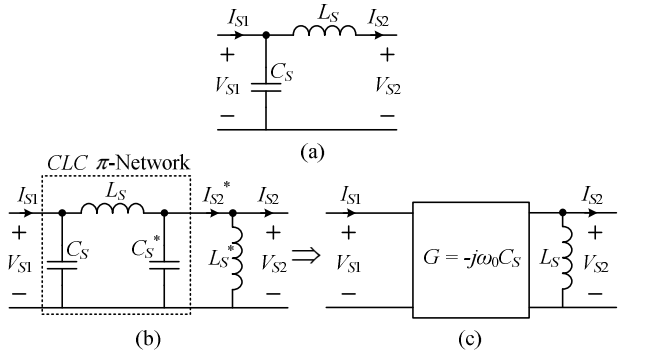

Fig. 3. Equivalent representations of parallel-series *LC* matching network: (a) L-type parallel-series resonant *LC* circuit; (b) Parallel resonator connected to the L-type circuit for π-type network arrangement; (c) Two-port network with gyrator characteristics.

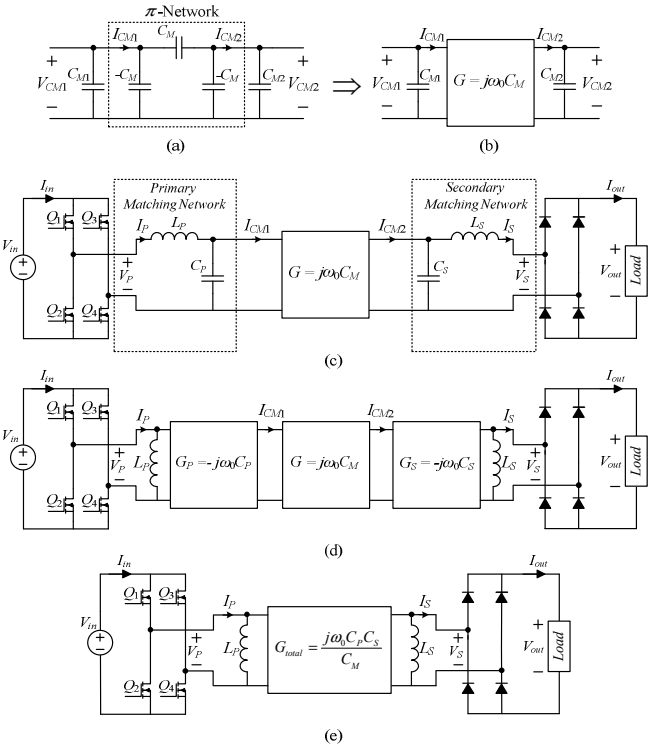

Fig. 5. Equivalent two-port network models of the capacitive WPT system: (a) Electrical equivalent model of four-plate capacitive medium; (b) Representation of the capacitive medium with a two-port network; (c) Representation of double-sided L-type capacitive WPT system with a gyrator as the capacitive medium;
(d) Equivalent circuit of double-sided L-type capacitive WPT system with three series gyrators; (e) Equivalent simplified circuit of double-sided L-type capacitive WPT system with a single gyrator.

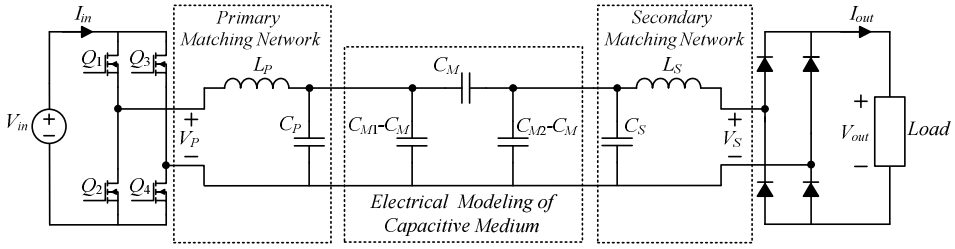

Fig. 4. Schematic diagram of a double-sided L-type capacitive WPT system.

gyrator, as illustrated in Fig. 5e, with total transconductance gain that can be expressed as

$$G_{total} = \frac{j\omega_0 C_P C_S}{C_M}. \quad (6)$$

The simplified circuit of the double-sided L-type capacitive WTP system in Fig. 5e can now be analyzed as a two-port network with gyrator characteristics, such that the current-voltage relationships are expressed as follows:

$$\begin{aligned} I_P &= \frac{V_P}{j\omega_0 L_P} - \frac{j\omega_0 C_P C_S}{C_M} V_S = -j\left(\frac{V_P}{\omega_0 L_P} + \frac{\omega_0 C_P C_S}{C_M} V_S\right) \\ I_S &= -\frac{V_S}{j\omega_0 L_S} + \frac{j\omega_0 C_P C_S}{C_M} V_P = j\left(\frac{V_S}{\omega_0 L_S} + \frac{\omega_0 C_P C_S}{C_M} V_P\right) \end{aligned}. \quad (7)$$

In the typical applications of this CPT system, the absolute values of V_P and V_S are of the same order, operating frequency is in the MHz range, the network parallel capacitance values are in the range of hundreds of pF, inductances are tens to hundreds μH, and the mutual coupling capacitance, C_M, is in the order of a few pF. As a result, the transfer relationship of the system can be simplified to generic expressions as follows:

$$\begin{aligned} I_P &= \frac{\omega_0 C_P C_S}{C_M} V_S \\ I_S &= \frac{\omega_0 C_P C_S}{C_M} V_P \end{aligned} \quad ; \quad \begin{cases} \frac{\omega_0 C_P C_S}{C_M} >> \frac{1}{\omega_0 L_{P/S}} \\ G \approx G_{total} = \frac{\omega_0 C_P C_S}{C_M} \end{cases}, \quad (8)$$

which is in excellent agreement with [16] and [18].

The above analysis reveals that the double-sided L-type capacitive WPT system can be modeled as a voltage-dependent current source (illustrated in Fig. 6). Employing the fundamental harmonic approximation [38], the average value of the output current $I_{out,AVG}$ is found as function of the trans-conductance gain and the input voltage V_{in} as follows:

$$I_{out,AVG} = \frac{8}{\pi^2} \frac{\omega_0 C_P C_S}{C_M} V_{in}, \quad (9)$$

thus, the average output power $P_{out,AVG}$ can be expressed as

$$P_{out,AVG} = \left(\frac{8}{\pi^2} \frac{\omega_0 C_P C_S}{C_M} V_{in}\right)^2 \cdot R_{Load}, \quad (10)$$

It can be noticed from the above analysis that for the double-sided L-type CPT system the output current (as well as the output power) are inversely proportional to the mutual coupling capacitance C_M.

To verify and show a proof-of-concept of the behavioral model, a cycle-by-cycle simulation test-bench for the analyzed CPT system has been constructed in PSIM. The input voltage is 70 V and the medium mutual capacitance C_M =6 pF, at resonant frequency f_0 ≈1.55 MHz for a load resistance of R_{Load} =15 Ω. The resonant operation has been obtained with asymmetrical matching parameters: LP =67 μH, CP =156 pF for the primary side, and LS =90 μH, CS =116 pF for the secondary side. Simulation results of the currents and voltages of the primary and secondary sides are shown in Figs. 7a and 7b, respectively, whereas the dashed lines show the behavioral model predictions. The obtained peak values of the currents are in good agreement with the theoretical predictions in (8), which further implies that the average output current, $I_{out,AVG}$, is as expected from (9).

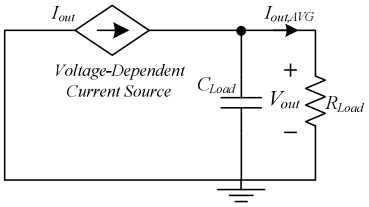

Fig. 6. Behavioral model of the analyzed capacitive WPT system for the output side.

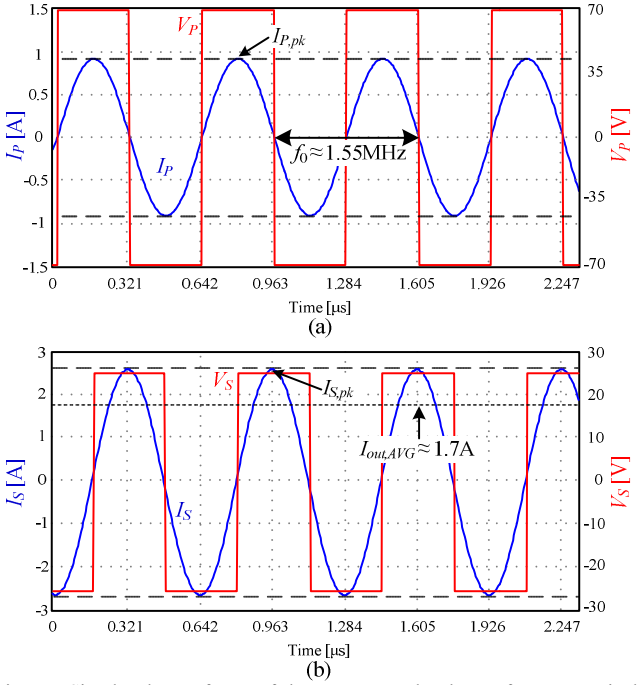

Fig. 7 Simulated waveforms of the currents and voltages for symmetrical matching parameters (dashed lines are the behavioral model predictions): (a) Primary, (b) Secondary.

IV. Simulation-Compatible Capacitive Medium Modeling

The coupling capacitance of the medium depends on various factors such as conductors, dielectric material, alignment and distance between the coupling plates. Evaluation of a WPT system in simulation environment for these variables over time or frequency is a major challenge, since a variable capacitance is required. To-date, this element is either absent from the common simulation software packages or very limited. Methods to obtain the medium characteristics either involve rigorous and tedious experiments and/or finite element analysis [19]. However, even in cases in which these characteristics are obtained, the analysis of their interaction with the electrical circuit is still required. To this end, a continuous-time model for variable capacitors, which can be extended to a variable-capacitance network model, has been developed and implemented in PSIM platform.

Several methodologies for continuous-time modeling of the non-linear effect of reactive components have been described in the literature. In particular, variable inductance with respect to self or auxiliary biasing has been described in [35], which has been later extended to variable capacitance [39], [40]. Since the description of variable capacitance is essential for CPT systems, this study extends the variable capacitance models,

originally employed for discrete components onto modeling of cross-coupled, capacitive network. As illustrated in Fig. 8, the model comprises dependent voltage and current sources, which emulate a non-linear transformer, and a capacitor with a reference capacitance. The characteristics of the non-linear transformer are defined by the following relationships:

$$\begin{aligned} V_2 &= K_{cap} V_1 \\ I_2 &= I_1 \end{aligned}, \tag{11}$$

where K_{cap} is the transformer's scale factor between the primary and secondary, and C_{ref} is the constant reference capacitance. From (11), the capacitive impedance reflected to the primary side, Z_C, with respect to the capacitive impedance at the secondary, Z_{Cref} is

$$\begin{cases} Z_C = \dfrac{1}{j\omega C} = \dfrac{V_1}{I_1} = \dfrac{V_2}{K_{cap} I_2} \\ Z_{Cref} = \dfrac{1}{j\omega C_{ref}} = \dfrac{V_2}{I_2} \end{cases} \Rightarrow \quad Z_C = \frac{1}{K_{cap}} Z_{Cref}, \tag{12}$$

and therefore, the capacitor value reflected to the primary side is obtained as

$$C = K_{cap} C_{ref} . \tag{13}$$

For the sake of simplicity, C_{ref} has been normalized to 1 F. In this case, the effective capacitance that is reflected across the capacitor terminals equals the scale factor K_{cap}. To evaluate a WPT system for continuous operation, K_{cap} can be made dependent on system parameters such as changes in distance and/or coupling capacitance, matching networks variations and mistuned resonant frequency. Thus, a voltage-dependent variable capacitor is emulated between nodes $C+$ and $C-$, as shown in Fig. 8.

To better view the implications of variations in the coupling capacitance and to observe sequential scenarios seamlessly, the two-port network model of the capacitive coupler has been also realized PSIM platform. This also allows to perform additional analysis of the system such as conditions for soft-switching, voltage and current stress, etc. The capacitive voltage-dependent current source I_{CM1} at the primary side of the coupler (Fig. 5) is generated as shown in Fig. 9 by replicating the current of an auxiliary capacitor, emulating the coupling capacitor C_M, which is exposed to the voltage V_{CM2}. In a similar manner, the capacitive voltage-dependent current source I_{CM2} at the secondary side of the coupler (Fig. 5) is generated by exposing another auxiliary coupling capacitor C_M to the voltage V_{CM1}. This enables to evaluate the CPT system in time-domain simulation, under different operating conditions, with a coupler model that includes the amplitudes, and more importantly, the phase shifts on-the-fly.

In order to evaluate the performance of a double-sided L-type system for continuous medium (distance) variations, based on the above-presented modeling technique, a simulation test-bench with variable capacitors has been constructed as shown in Fig. 10. There, for convenience the capacitive medium is illustrated by variable capacitor symbols. Simulations have been carried out under nominal operating conditions and matching networks that are identical to case study in Section III, whereas the initial coupling capacitance is 3.5 pF. Fig. 11a shows the changes in the average value of I_{out} for a 2.5 pF increase of the mutual capacitance, such that the final coupling capacitance is C_M=6 pF. The solid red line shows the simulation result, whereas the dashed blue line show the behavioral model outcome. It can be observed that the results of the cycle-by-cycle simulation and behavioral model are in a very good agreement. It can be further noticed that when C_M increases, the output current decreases as expected from the theoretical analysis. Fig. 11b shows the output current for a 1.5pf step-down variation of the coupling capacitance, such that its final value is C_M=2 pF. The output current settles on approximately 5 A for both the model and cycle-by-cycle simulation, which suits well the theoretical predictions.

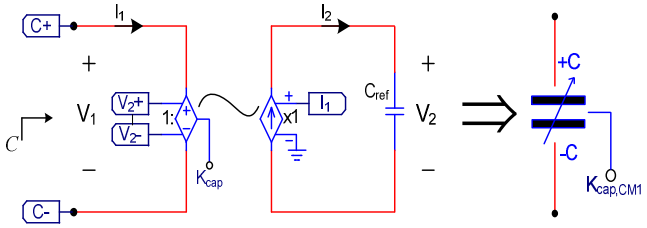

Fig. 8 Continuous variable capacitor model in PSIM platform.

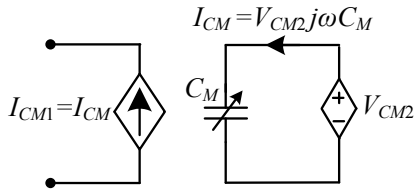

Fig. 9 Capacitive coupler equivalent simulation-compatible electrical model.

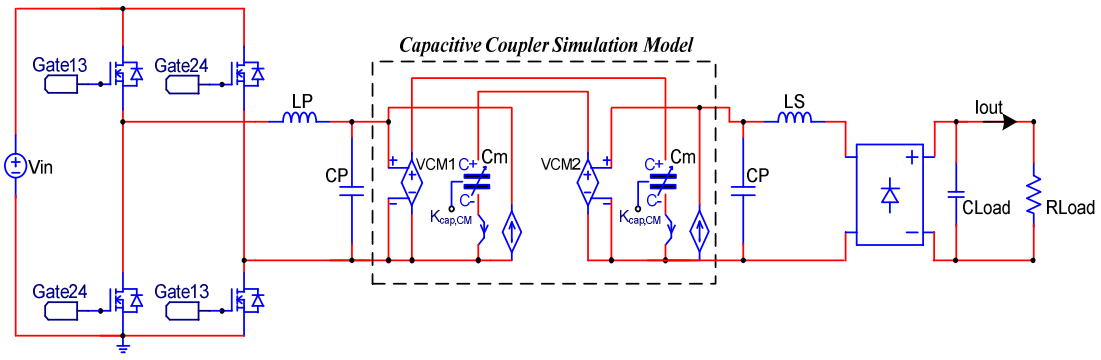

Fig. 10 Schematic simulation test-bench of the WPT system with variable capacitor symbol illustrations for the mutual capacitance.

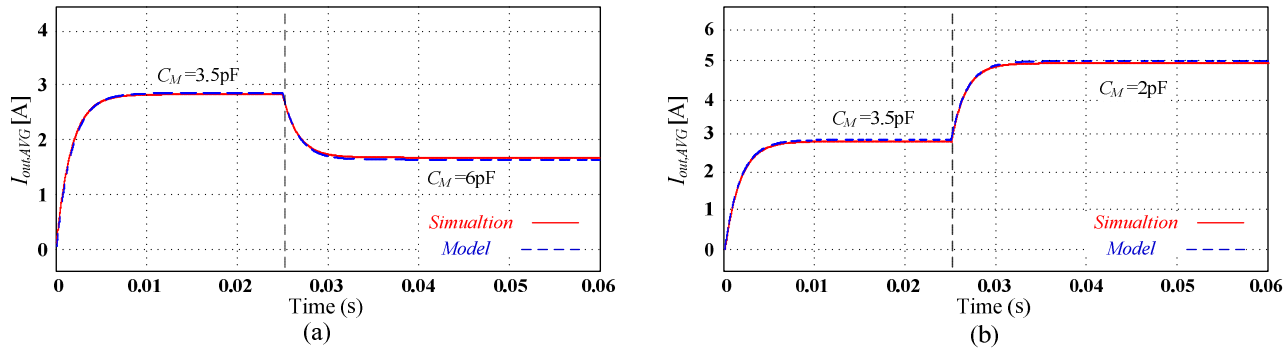

Fig. 11 Average output current for capacitive medium variations with initial mutual capacitance C_M = 3.5pF. (a) Step-up of 2.5pF, (b) Step-down of 1.5pF.

V. Experimental Validation

To validate and examine the model predictions, an experimental double-sided L-type capacitive WPT prototype with four copper plates, that form the capacitive coupling, has been constructed as shown in Fig. 12. The coupling plates have been designed symmetrically, such that each plate is 17x17 cm. Thus, the matching networks have been also designed to be symmetrical, with L_P=L_S≈67 µH and C_P=C_S =156 pF. The full-bridge inverter has been implemented with GaN modules operated at several MHz, and the gate drive signals were generated with a Cyclone IV FPGA at an operating frequency slightly above the resonance f_0 ≈1.558 MHz guaranteeing soft-switching operation. To operate in the MHz range without any concern nor limitation due to magnetic and skin-effect losses, the matching inductors L_P and L_S have been constructed with a litz wire wrapped on an air-core. High-voltage multilayer SMD ceramic capacitors have been used for the matching capacitors C_P and C_S. The overall operating conditions and parameters of the experimental prototype are summarized in Table I.

Fig. 13 shows experimental waveforms of the system for an air-gap of 30 mm (corresponds to C_M ≈5 pF approximately), whereas the input voltage V_{in}=30 V and the load resistance R_{Load} ≈15 Ω. Fig. 13a shows the primary waveforms, as can be seen V_P toggles between -30 V to 30 V and the peak value of the sinusoidal current I_P is ~1.22 A. The current at the secondary, I_S, is shown in Fig. 13b, the obtained peak value (1.8 A) as well as the resulting average value (~1.1 A) are in a very good agreement with (8) and (9), respectively. Fig. 14 shows experimental waveforms for an air-gap of 60 mm which corresponds to C_M of 3 pF approximately. The measured output voltage and current suit well the theoretical predictions. Additionally, as can also be observed from Fig. 14b, the output current increases as the coupling decreases, validating the inversely proportional relationship between C_M and output current, as well as the output power.

TABLE I – Experimental Prototype Values and Parameters

Parameter	*Value/Type*
Input voltage V_{in}	30 V
Load resistance R_{Load}	15 Ω
Coupling plates	17x17 cm
Air-gaps	30~60 mm
Full-bridge transistors	LMG5200, 80 V, 15 mΩ
Inductors L_P and L_S	~67 µH
Capacitors C_P and C_S	156 pF
Resonant frequency f_0	1.5 MHz

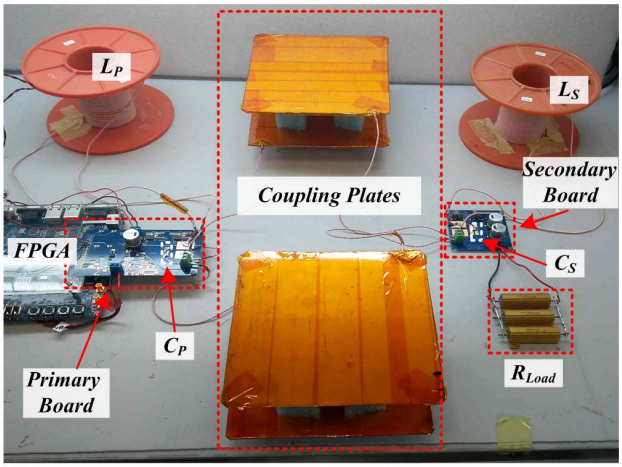

Fig. 12 Experimental setup of a capacitive WPT prototype.

To further validate the behavioral model, the average output current has been measured for various input voltages, for a constant air-gap of 30 mm, the results are summarized in Fig. 15. The model predictions as well as the simulation results tightly follow the experimental measurements. It can be noticed that the output current increases with the input voltage, as predicted from the gyrator current-voltage relationships obtained in Section III.

VI. Conclusion

A generic network-based modeling approach for resonant capacitive WPT systems has been presented. Based on the modeling approach, the behavior of resonant-operating CPT system can be analyzed and described for different system variations such as capacitive coupling interface, resonant frequency and matching networks components. The modeling method provides an insight to the effects of the parameters on the system behavior, the cross-coupling relationships between transmitter and receiver sides based on the operation mode and settings. This study also introduced a simulation-compatible capacitive medium model followed by a variable capacitor model that is applicable for continuous-time analysis of WPT systems. An experimental double-sided L-type CPT prototype has been designed and examined in the MHz range to validate the theoretical framework. Various measurements up to 60 mm air-gap have been carried out, and the results are in an excellent agreement with the theoretical analysis and simulations.

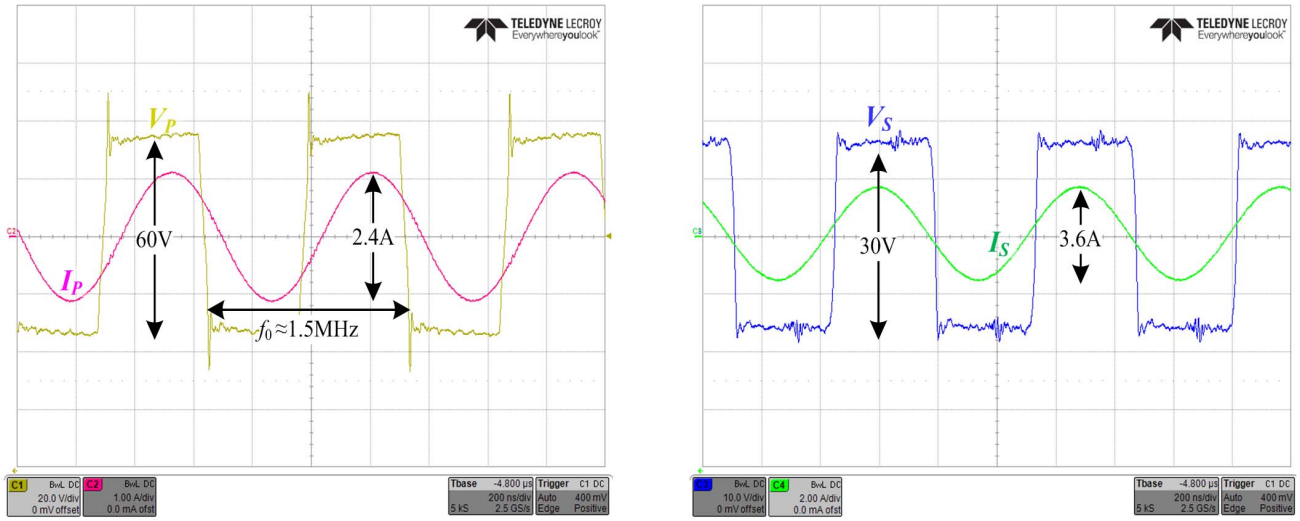

Fig. 13 Experimental waveforms with operating conditions: V_{in} =30 V, R_{Load} =15 Ω, coupling capacitance C_M ≈5 pF. (a) Primary side V_P 20V/div, I_P 1A/div, (b) Secondary side V_S 10V/div, I_S 2A/div. Time scale 200ns/div.

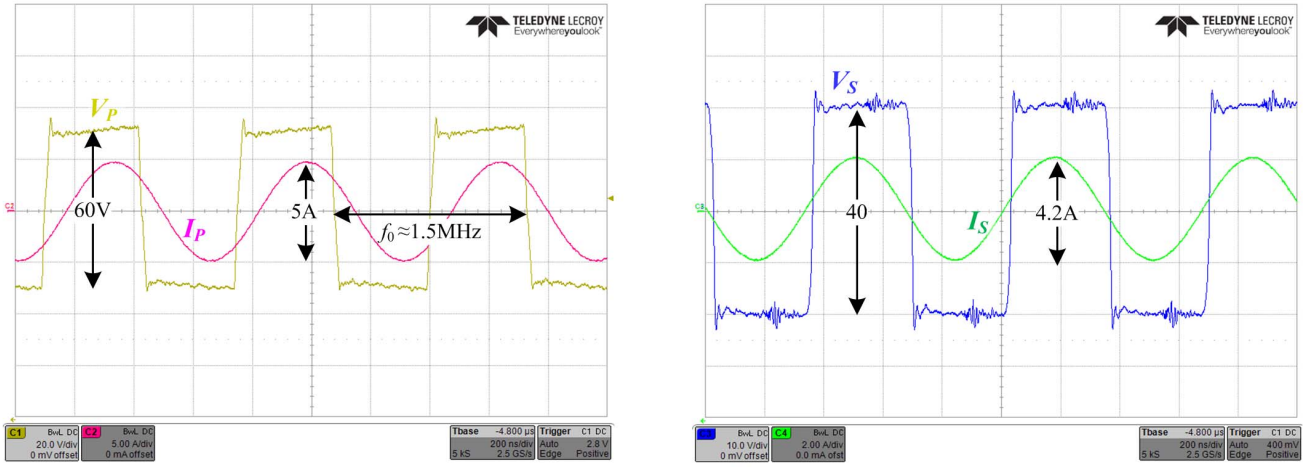

Fig. 14 Experimental waveforms with operating conditions: V_{in} =30 V, R_{Load} =15 Ω, coupling capacitance C_M ≈3 pF. (a) Primary side V_P 20V/div, I_P 5A/div, (b) Secondary side V_S 10V/div, I_S 2A/div. Time scale 200ns/div.

ACKNOWLEDGEMENT

This research was supported by the Pazi foundation.

REFERENCES

[1] T. Imura and Y. Hori, "Maximizing air gap and efficiency of magnetic resonant coupling for wireless power transfer using equivalent circuit and Neumann formula," *IEEE Trans. Ind. Electron*., vol. 58, no. 10, pp. 4746–4752, Oct. 2011.

[2] P. Si, A. P. Hu, S. Malpas, D. Budgett, "A frequency control method for regulating wireless power to implantable devices," *IEEE Trans. on Biomedical Circuits and Systems*., vol. 2, no. 1, pp. 22– 29, March. 2008.

[3] T. Langlotz, T. Nguyen, D. Schmalstieg, and R. Grasset, "Next generation augmented reality browsers: Rich, seamless, and adaptive," in *Proc. IEEE*, vol. 102, no. 2, pp. 155–169, Feb. 2014.

[4] J. Sallan, J. L. Villa, A. Llombart, and J. F. Sanz, "Optimal design of ICPT systems applied to electric vehicle battery charge," *IEEE Trans. Ind. Electron*., vol. 56, no. 6, pp. 2140–2149, Jun. 2009.

[5] D. Yin, S. Oh, and Y. Hori, "A novel traction control for EV based on maximum transmissible torque estimation," *IEEE Trans. Ind. Electron*., vol. 56, no. 6, pp. 2086–2094, Jun. 2009.

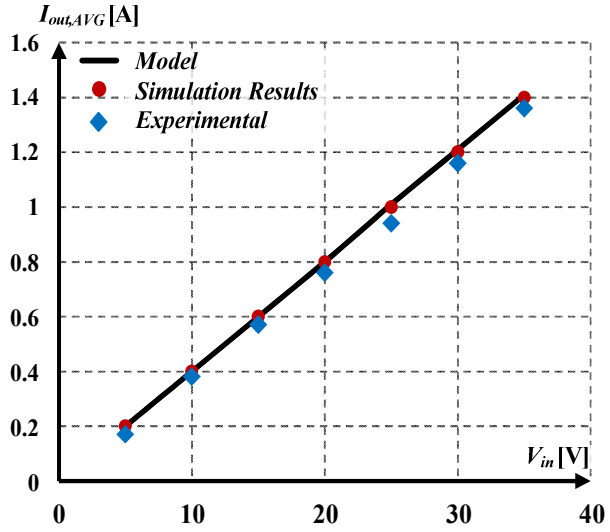

Fig. 15 Average output current, $I_{out,AVG}$, curve as function of the input voltage for 30 mm air-gap.

[6] S. Li and C. Mi, "Wireless Power Transfer for Electric Vehicle Applications," *IEEE Journal of Emerging and Selected Topics in Power Electronics*, vol. PP, pp. 1-1, 2014.

[7] S. Jaegue et al., "Design and implementation of shaped magnetic resonance-based wireless power transfer system for roadway-powered moving electric vehicles," *IEEE Trans. Ind. Electron*., vol. 61, no. 3, pp. 1179–1192, Mar. 2014.

[8] K. Wu, D. Choudhury, and H. Matsumoto, "Wireless power transmission, technology, and applications" *Proceedings of the IEEE*, Vol. 101, no.6, pp. 1271 – 1275, June 2013.

[9] L. Collins, "Cut the cord," *IET Journals & Magazines.*, vol. 5, no. 6, pp. 42–46, Jan.–Dec. 2007.

[10] V. Valente, et al., "A high-power CMOS class-D amplifier for inductive link medical transmitters," *IEEE Trans. Power Electron.,* vol. 30, no. 8, pp. 4477–4488, Aug. 2015.

[11] S.Y.R. Hui, W. Zhong and C.K. Lee, "A critical review of recent progress in mid-range wireless power transfer," *IEEE Transactions on Power Electronics*, vol. 29, no. 9, pp. 4500–4511, September 2014.

[12] F. Musavi and W. Eberle, "Overview of wireless power transfer technologies for electric vehicle battery charging," *IET Power Electronics*, vol. 7, no. 1, pp. 60–66, 2014.

[13] M. P. Theodoridis, "Effective capacitive power transfer," *IEEE Trans. Power Electron*., vol. 27, no. 12, pp. 4906–4913, Dec. 2012.

[14] F. Lu, H. Zhang, H. Hofmann, and C. Mi, "A double-sided LCLC compensated capacitive power transfer system for electric vehicle charging," *IEEE Trans. Power Electron.*, vol. 30, no. 11, pp. 6011–6014, Jun. 2015.

[15] H. Zhang, F. Lu, H. Hofmann, W. Liu, and C. C. Mi, "A four-plate compact capacitive coupler design and LCL-compensated topology for capacitive power transfer in electric vehicle charging application," *IEEE Trans. Power Electron*., vol. 31, no. 12, pp. 8541–8551, Dec. 2016.

[16] F. Lu, H. Zhang, H. Hofmann, C. Mi, "A loosely coupled capacitive power transfer system with LC compensation circuit topology," *Proc. IEEE Energy Convers. Congr. Expo. (ECCE)*, pp. 1–5, 2016.

[17] F. Lu, H. Zhang, C. Mi, "A two-plate capacitive wireless power transfer system for electric vehicle charging applications," *IEEE Trans. Power Electron*, vol. 33, no. 2, pp. 946–969, Aug. 2017.

[18] F. Lu, H. Zhang, H. Hofmann, and C. Mi, "A double-sided LC compensation circuit for loosely-coupled capacitive power transfer," *IEEE Trans. Power Electron*., vol. 33, no. 2, pp. 1633 – 1643, Feb. 2017.

[19] J. Dai and D.C Ludois, "A survey of wireless power transfer and a critical comparison of inductive and capacitive coupling for small gap applications," *IEEE Trans. Power Electron*, vol. 30, no. 11, pp. 6017-6029, Nov. 2015.

[20] F. Lu, H. Zhang, H. Hofmann, C. Mi, "An inductive and capacitive integrated coupler and its LCL compensation circuit design for wireless power transfer," *IEEE Trans. Industry Applications*, vol. 53, no. 5, pp. 4903–4913, Oct. 2017.

[21] W. Zhang and C. Mi, "Compensation topologies for high power wireless power transfer systems," *IEEE Transactions on Vehicular Technology*, vol. 65, no.6, pp. 4768-4778, July 2015.

[22] S. Sinha, A. Kumar, S. Pervaiz, B. Regensburger and K.K. Afridi, "Design of efficient matching networks for capacitive wireless power transfer systems," *Proceedings of the IEEE Workshop on Control and Modeling for Power Electronics (COMPEL)*, Trondheim, Norway, June 2016.

[23] A. Kumar, S. Sinha, A. Sepahvand, K. K. Afridi, "Improved design optimization for high-efficiency matching networks," *IEEE Transactions on Power Electronics*, vol. 33, no. 1, pp. 37-50, Jan 2018.

[24] Z. Pantic, B. Sanzhong, and S. Lukic, "ZCS LCC-compensated resonant inverter for inductive-power-transfer application," *IEEE Trans. Ind. Electron.*, vol. 58, no. 9, pp. 3500–3510, Aug. 2011.

[25] A. Witulski and R. W. Erickson, "Extension of state-space averaging to resonant switches and beyond," *IEEE Trans. Power Electron.*, vol. 5, no. 1, pp. 98–109, Jan. 1990.

[26] H. Hao, G. A. Covic, and J. T. Boys, "An approximate dynamic model of LCL-T-based inductive power transfer power supplies," *IEEE Trans. Power Electron*., vol. 29, no. 10, pp. 5554–5567, Oct. 2014.

[27] V. Vorperian, R. Tymerski, and F. C. Lee, "Equivalent circuit models for resonant and PWM switches," *IEEE Trans. Power Electron*., vol. 4, no. 2, pp. 205–214, Apr. 1989.

[28] D. Maksimovic and S. Cuk, "A unified analysis of PWM converters in discontinuous modes," *IEEE Trans. Power Electron*., vol. 6, no. 3, pp. 476–490, Jul. 1991.

[29] J. Lu, A. Kumar, K. K. Afridi, "A step-superposition based analysis approach to modeling resonant converters," *IEEE Trans. Power Electron*., vol. 33, no. 8, pp. 7148-7165, Aug. 2018.

[30] C. J. Anderson and J. A. Lyle, "Technique for evaluating system performance using Q in numerical simulation exhibiting inter symbol interference," *Electron. Lett*., vol. 30, pp. 71–72, 1994.

[31] L. Chen, S. Liu, Y. Zhou, and T. Cui, "An optimizable circuit structure for high-efficiency wireless power transfer*," IEEE Trans. Ind. Electron.*, vol. 60, no. 1, pp. 339–349, Jan. 2013.

[32] B. Wang, W. Yerazunis, and K. H. Teo, "Wireless power transfer: Metamaterials and array of coupled resonators," in *Proc. IEEE*, vol. 101, no. 6, pp. 1359–1368, Jun. 2013.

[33] Q. Yuan, Q. Chen, L. Li, and K. Sawaya, "Numerical analysis on transmission efficiency of evanescent resonant coupling wireless power transfer system," *IEEE Trans. Antennas Propag*., vol. 58, no. 5, pp. 1751–1758, May 2010.

[34] C. Lin and F. Lee, "Design of a piezoelectric transformer converter and its matching networks," *Proc. IEEE-PESC'94 Conf*., vol. 1, pp. 607–612, 1994.

[35] S. Ben-Yaakov and M.M. Peretz, "Simulation bits: A SPICE behavioral model of non-linear inductors," *IEEE Power Electron. Soc.Newslett*., vol. 15, no. 4, pp. 9–10, 4th Quarter 2003.

[36] Y. H. Sohn, B. H. Choi, G. H. Cho, and C. T. Rim, "Gyrator-based analysis of resonant circuits in inductive power transfer systems," *IEEE Transactions on Power Electronics*, vol. 31, no. 10, pp. 6824-6843, Oct. 2016.

[37] A. Cid-Pastor, L.Martinez-Salamero, C. Alonso, R. Leyva, and S. Singer, "Paralleling DC–DC switching converters by means of power gyrators," *IEEE Trans. Power Electron.*, vol. 22, no. 6, pp. 2444–2453, Nov. 2007.

[38] R.L. Steigerwald, "A comparison of half-bridge resonant converter topologies," *IEEE Transactions on Power Electronics*, vol. 3, no. 2, pp. 174-182, April 1988.

[39] M. Evzelman and M. M Peretz "Optimal design of a class-E resonant driver," *IET Power Electronics,* vol. 8, no.8, pp 1552-1557, Apr. 2015.

[40] I. Zeltser and S. Ben-Yaakov, "On SPICE simulation of voltage-dependent capacitors," *IEEE Transactions on Power Electronics*, vol. 33, no. 5, pp. 3703-3710, Oct. 2017.